Geophysical Research Letters

RESEARCH LETTER
10.1029/2025GL119013

Influence of Mesoscale Organization on the Formation of Humidity Haloes

Marius Rixen[1,2], **Julia Windmiller**[1], **and Bjorn Stevens**[1]

[1]Max-Planck Institute for Meteorology, Hamburg, Germany, [2]ETHZ, Zürich, Switzerland

Key Points:

- Ground-based LiDAR shows trade cumulus clouds have humidity haloes with a radiative effect of 0.68 Wm^{-2}, spreading horizontally up to 9 km
- A mass flux estimation reveals that detrainment from clouds is unlikely to be the only factor responsible for causing these humidity haloes
- Humidity haloes are tied to mesoscale cloud organization and clustering, suggesting a self-reinforcing relationship

Correspondence to:
M. Rixen,
marius.rixen@env.ethz.ch

Citation:
Rixen, M., Windmiller, J., & Stevens, B. (2025). Influence of mesoscale organization on the formation of humidity haloes. *Geophysical Research Letters*, *52*, e2025GL119013. https://doi.org/10.1029/2025GL119013

Received 31 AUG 2025
Accepted 13 NOV 2025

Author Contributions:
Conceptualization: Julia Windmiller, Bjorn Stevens
Data curation: Marius Rixen
Formal analysis: Marius Rixen
Investigation: Marius Rixen, Julia Windmiller, Bjorn Stevens
Methodology: Marius Rixen, Julia Windmiller, Bjorn Stevens
Resources: Julia Windmiller
Software: Marius Rixen
Supervision: Julia Windmiller, Bjorn Stevens
Visualization: Bjorn Stevens
Writing – original draft: Marius Rixen
Writing – review & editing: Marius Rixen, Julia Windmiller, Bjorn Stevens

Abstract Humidity haloes-regions of enhanced water vapor surrounding trade wind shallow cumulus clouds-can significantly influence downward longwave radiation due to their elevated moisture content compared to clear-sky conditions. Using data from the Barbados Cloud Observatory—including longwave radiation measurements and moisture profiles from the co-located CORAL LiDAR instrument—we analyze the radiative environment around clouds. After observing such humidity haloes up to a distance of 9 km from shallow cumulus clouds, we find an average increase in downward longwave radiation due to haloes of 0.68 W m^{-2}, which is consistent with previous satellite based observational estimates. The cause of halo formation is also examined. A rough mass flux estimate suggests detrainment from a single cloud alone can't explain their formation. Our results suggest that mesoscale organization likely plays a key role in modulating moisture in the boundary layer and especially at cloud level, thus contributing to increasing humidity around clouds.

Plain Language Summary Shallow cumulus clouds in the trade winds are often surrounded by regions of increased humidity, called humidity haloes. These haloes affect the climate by increasing the amount of longwave radiation trapped on Earth. Using ground-based observations from the Barbados Cloud Observatory, we measured this effect and found that these haloes can extend horizontally up to 9 km from the cloud and enhance radiation by 0.68 W m^{-2} as previously found in satellite observations. These haloes were previously thought to result from moisture detrained from the respective cloud. However, we show that this explanation alone is insufficient. Instead, mesoscale clustering of clouds could play a key role in shaping humidity patterns at cloud level.

1. Introduction

Significant enhancement of humidity has been observed around shallow trade wind cumulus clouds, forming so-called humidity haloes (Eytan et al., 2020; Jahani et al., 2020; Malkus, 1954; Perry & Hobbs, 1996). These haloes —also referred to as transition zones, humidity shells, or twilight zones—show elevated relative humidity compared to the surrounding clear-sky environment. Humidity in the environment of a cloud can impact the cloud because it can inhibit the generation of negative buoyancy during mixing, as cloud buoyancy strongly depends on the humidity of the entrained air. Moreover, accurate computation of radiative fluxes, especially in the longwave spectrum, requires precise representation of water vapor due to its strong influence on radiative transfer (Bar-Or et al., 2012; Pinsky & Khain, 2019). Eytan et al. (2020) used 1 km resolution satellite data of brightness temperature to detect humidity haloes extending up to 11 km from clouds, showing that their radiative impact decays exponentially with distance. On average, they reported a longwave radiative forcing of 0.75 W m^{-2} caused by these humidity anomalies. They propose that these humidity haloes constitute a distinct atmospheric regime, rather than simply categorizing regions as either cloudy or clear sky. Overlooking this can introduce substantial errors in estimating cloud radiative effects, which play a crucial role in evaluating clouds' impact on Earth's radiation energy budget.

The processes responsible for the formation of these haloes, however, remain uncertain. The prevailing explanation is the cloud itself moistens its environment (e.g., via detrainment) (Gu et al., 2021; Lu et al., 2012; Perry & Hobbs, 1996; Pinsky & Khain, 2019; Wang & Geerts, 2010). Yet, it seems implausible that a single shallow cumulus cloud alone could detrain enough moisture to affect the environment up to 11 km away. This raises the possibility that another mechanism modulates moisture in the lower atmosphere. One such hypothesis was put forward by George et al. (2023), who identified Shallow Mesoscale Overturning Circulations in the trade winds. These circulations span length scales from $\mathcal{O}(10)$ km to $\mathcal{O}(100)$ km and are associated with significant mesoscale

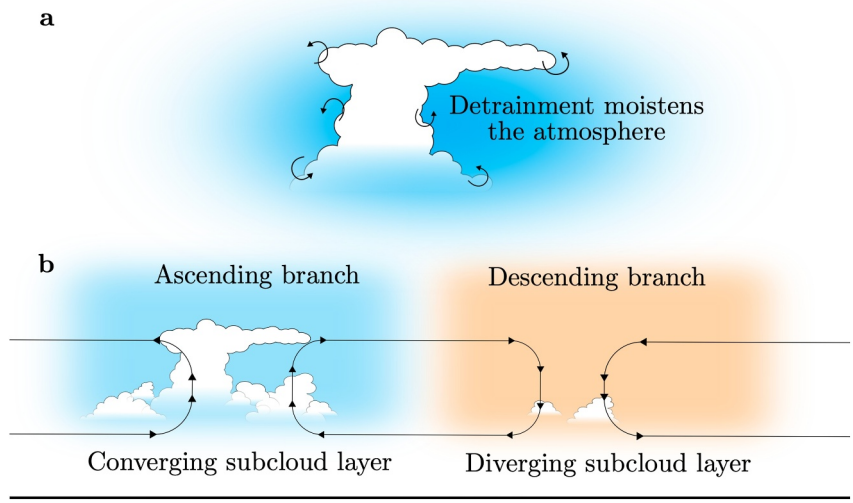

Figure 1. Schematic of the two hypothesis for moisture variation around clouds. Panel (a) depicts the prevailing view, where haloes result from clouds detrainment. Panel (b) presents an alternative perspective in which humidity variations are shaped by broader mesoscale organization or clustering within the boundary layer. In this framework, moist ascending regions (blue) and dry descending regions (brown) emerge as part of a larger-scale pattern that influences where clouds preferentially form. Panel (b) was adapted based on George et al. (2023).

variability in vertical velocity and moisture at cloud base. Such mesoscale organization could influence the efficiency of moistening and drying throughout the boundary layer, shaping where clouds preferentially form. In this view, elevated water vapor around clouds could reflect broader patterns of organization, rather than being solely a by-product of individual clouds. More generally, humidity anomalies surrounding clouds may both result from and contribute to cloud clustering. Regions of enhanced humidity can favor repeated cloud formation, while clustered clouds may in turn reinforce local moistening. These two conceptual mechanisms—cloud-driven moistening and pre-existing organization—are illustrated schematically in Figure 1.

We analyze observations of fair-weather clouds to identify humidity haloes and assess their radiative impact, confirming consistency with satellite-based findings by Eytan et al. (2020). Using Barbados Cloud Observatory (BCO) data, we estimate updraft mass fluxes to evaluate moisture detrainment and examine vertical humidity profiles to explore how cloud clustering and mesoscale organization modulate humidity variability around clouds. Our use of vertically resolved data provides insight into the origin and structure of humidity enhancements near clouds.

2. Data

In this study, data from the BCO is used (Stevens et al., 2016), a facility managed by the Max Planck Institute for Meteorology and the Caribbean Institute for Meteorology and Hydrology since April 2010. Situated atop a 17-m promontory on Barbados' Deebles Point (13.16°N, 59.43°W), the BCO captures largely undisturbed Atlantic trade-wind conditions due to its location. Clouds at the BCO are representative of clouds across the trade wind regions in observations and in climate models (Medeiros & Nuijens, 2016). Therefore, this observatory stands as a natural laboratory for trade wind clouds. Our data set comprises surface meteorology, radiant energy measurements, cloud radar data, and Doppler LiDAR data from the year 2020.

Downward longwave diffuse radiation (LW↓) is measured using a shaded pyrgeometer with a temporal resolution of 1 s, averaged to 1 min to reduce background noise. The Ka-band cloud radar provides radar reflectivity every 10 s with a vertical resolution of approximately 30 m. From this reflectivity, a cloud mask is derived following Konow (2020), using a defined threshold to identify shallow cumulus clouds. The Raman LiDAR delivers high-resolution water vapor profiles (4 s time window) up to 3 km altitude. Since our focus is on shallow cumulus clouds, we restrict the analysis to the lowest 2 km. Figure 2 summarizes the key measurements from both instruments during the passage of a cloud over the BCO. Visual inspection of numerous clouds reveals features

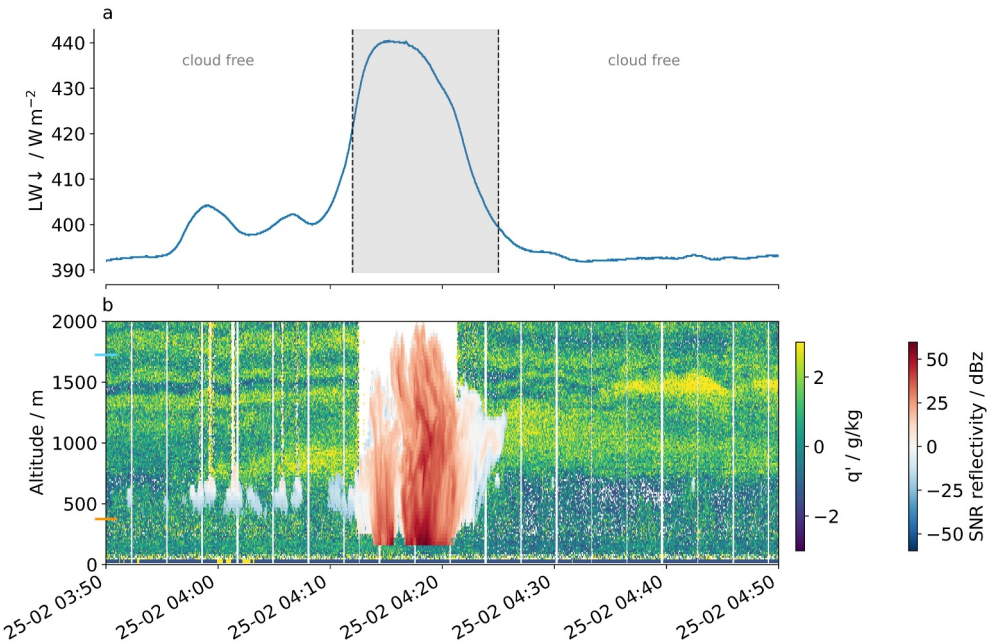

Figure 2. Example for one cloud passing over the Barbados Cloud Observatory on 25th of February 2020. Panel (a) shows the emitted downward longwave radiation. Black dashed vertical lines denote the cloud boundaries and the shaded region indicates the cloud interior. Panel (b) displays the reflectivity Signal to Noise Ratio from the radar as well as the specific humidity anomaly q' from the LiDAR. Note that the LiDAR does not penetrate through thick clouds and therefore NaN values are measured above the cloud base for q' measurements. The orange tick marks the cloud base layer, while the light blue tick indicates the inversion layer height.

similar to those illustrated in Figure 2, with a clear increase in downward longwave radiation within the cloud boundaries and a decrease around the cloud. The right-hand decay appears sharp, while the left side is bumpier, likely caused by very small cloud fragments with low reflectivity that are not captured by the cloud mask. These subcloud features likely produce a more gradual decrease in radiation. Laminated moist structures are resolved by the high vertical resolution of the Raman LiDAR; however, unlike the broader humidity haloes, these are not robust features but vary from cloud to cloud. The analysis therefore emphasizes the large-scale moisture decay with distance from clouds rather than these smaller-scale variations.

This example highlights the high variability of the radiative response around clouds, while the focus of this study is on the overall mean effect.

3. Observations of Clouds From Downward Longwave Radiation

3.1. Methods: Downward Longwave Radiation Composite

To study humidity haloes, radiant energy measurements and cloud mask data are used. The start and end times of each cloud during our time series are extracted from the cloud mask. Following Jung et al. (2016) and Lonitz (2014), shallow cumulus clouds with depths less than 700 m are selected to restrict the analysis to shallow convection and avoid influence from deeper clouds. To avoid cross-contamination—that is, to ensure that the downward longwave radiation (LW↓) attributed to a given cloud is not influenced by the high LW↓ values inside nearby clouds—we set the emissions from all clouds to NaN (to keep the emission from each cloud' surrounding only). For each cloud, we retain the LW↓ data only within a time window of 50 min before and 50 min after the cloud's passage, which we call a cloud array. The filtered radiation data are averaged as a function of distance to the nearest cloud edge, with time converted to distance using windspeed measurements averaged over the corresponding time period.

To quantify the effect of humidity haloes on the LW↓, the RE is computed similarly to Eytan et al. (2020). To remove synoptic variability, the minimum LW↓ of each cloud array is subtracted from the measured emission:

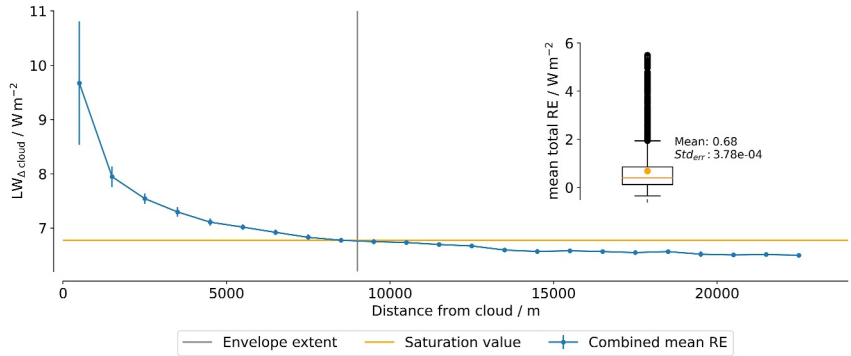

Figure 3. Composite of $LW_{\Delta cloud}$ as a function of distance from all shallow cumulus clouds in 2020, binned every 1000 m. The errors bars represent the standard error, the orange line marks the saturation level (clear-sky emission), and the gray vertical line indicates the halo extent where saturation is reached. The inset box plot shows the distribution of total radiative effect, with the orange dot as the mean and orange bar as the median.

$$LW_{\Delta\,cloud} = LW\downarrow - \min(LW_{cloud}) \quad (1)$$

where $\min(LW_{cloud})$ is the minimum measured value for each cloud array. The RE can be computed as follows:

$$RE = LW_{\Delta\,cloud} - LW_{clear\ sky} \quad (2)$$

where $LW_{clear\ sky}$ is the value of LW↓ in a (relatively) dry environment, that is, in clear sky conditions. This is defined as the value of LW↓ where the decay with distance is close to saturation (referring to the distance at which LW↓ no longer changes with increasing distance from the cloud). We also use this distance to mark the maximum extent of the humidity envelope.

3.2. Results

Following Eytan et al. (2020), Figure 3 shows a composite of $LW_{\Delta\,cloud}$ (see Equation 1) averaged over all observed shallow cumulus clouds. This figure illustrates the increase in incoming longwave radiation toward clouds boundaries. The longwave emission shows a gradual increase over more than 10 km, followed by a very sharp rise near the cloud. Without the presence of a halo, we would not expect to observe this gradual increase of LW↓. This result indicates that cloud haloes are observable in trade wind clouds through LW↓ measurements in agreement with Gonzalez et al. (2023).

From this figure, we derive the extent of humidity haloes. We first identify the saturation value, that is, the clear-sky LW↓, defined as the distance where the $LW_{\Delta\,cloud}$ decreases by less than a defined cutoff threshold of 0.05 W m^{-2} at each following bin. The saturation value is reached up to a distance of 9 km, meaning that haloes are observed up to 9 km. Following Equation 2, the RE of all shallow cumulus cloud haloes is computed by averaging the signal. The box-plot in Figure 3 shows the distribution of the total effect for all shallow cumulus clouds. Although the values show considerable variability (as indicated by the outliers in the box plot), the error remains small due to the large sample size—approximately 17,000 shallow clouds were observed. Here we use the standard error of the mean to report the error which is given as the standard deviation divided by the square roots of number of samples. The mean value of $RE_{shallow} = 0.68$ W m^{-2} means that on average, cloud haloes enhance the LW↓ by 0.68 W m^{-2}. Sensitivity tests with different cutoff thresholds confirm the robustness of this estimate: varying the threshold from 0.01 to 0.1 W m^{-2} changes the mean RE only slightly from 0.71 to 0.67 W m^{-2}. This indicates that the derived halo effect is not strongly dependent on the exact cutoff choice. Furthermore, the cumulative RE increases rapidly within the first few kilometers from the cloud edge (not shown), with about 80% of the total effect reached within 5 km, indicating that small variations in halo extent have only a minor influence on the total LW↓ enhancement.

Our value of 0.68 W m^{-2} is very close to the value found by Eytan et al. (2020), in which they computed a mean RE of 0.75 W m^{-2} which shows a consistency in these results. The approximate 10% discrepancy between these

two values may stem from the different methodologies: while Eytan et al. (2020) relied on satellite observations, our analysis is based on ground-based in situ remote sensing using LiDAR. In particular, Eytan et al. (2020) used global, multi-day satellite coverage, whereas our study represents detailed observations from a single, well-instrumented site, highlighting both a difference in spatial scale and sampling approach. The conditions at the BCO during our study period were broadly representative of typical trade-wind regimes whereas (Eytan et al., 2020) sampled shallow clouds in different environments.

4. Influence of Mesoscale Organization in Modulating the Moisture Variance at Cloud-Level

4.1. Mass Flux Estimation

The observation of cloud haloes extending up to 9 km is surprising, as the physical processes thought to generate such humidity enhancements—detrainment, cloud-edge mixing, and evaporative cooling—typically act over shorter ranges. To test whether detrainment alone can explain the observed humidity haloes, we use a simple mass flux model to estimate the potential increase in humidity from a single cloud. In this approach, we approximate the amount of moisture transported upward by an updraft and assume that the entire cloud detrains into the environment. This provides an upper-limit estimate of the possible moistening effect from one cloud. Detrainment efficiency is expected to vary with the cloud life-cycle, with mature clouds typically detraining more moisture than developing or decaying ones. As our analysis does not include information on individual cloud ages, we therefore average over all observed clouds, effectively integrating across different life-cycle stages. The estimation is carried out as follows. The amount of moisture advected by an updraft is approximated as:

$$M_{\mathrm{wv}} = w \cdot q_{\mathrm{BL}} \cdot A \cdot \tau \cdot \rho \tag{3}$$

where w is the vertical velocity, q_{BL} the humidity in the boundary layer, A the area of the updraft, τ the typical lifetime of a cloud, set to 30 min (Siebesma et al., 2003), and ρ the air density given by the barometric formula. w is taken as the 90th% quantile of the observed upward velocity at the BCO, which is $w = 2.88\,\mathrm{ms}^{-1}$. Both τ and w are chosen conservatively high, likely providing an upper bound in the estimation. The area is computed from the mean length of the observed shallow cumulus clouds which is approximately 500 m. The humidity is derived from surface measurements of pressure, temperature, and relative humidity, using the following formula:

$$q = 0.622 \cdot \frac{e}{P - 0.378 \cdot e} \tag{4}$$

where P is the pressure in Pa, e the partial water vapor pressure in Pa. Using the same approach as for the vertical velocity, the 90th percentile of the computed surface humidity is $q_{\mathrm{BL}} = 16.59\,\mathrm{g\,kg}^{-1}$. From these parameters, the estimated upward-moisture reaches about $M_{\mathrm{wv}} \approx 1.95 \cdot 10^{10}\,\mathrm{kg}$.

To compare with the moisture in the atmosphere around the halo, the halo is approximated as a cylinder surrounding the cloud. The selected shallow clouds have an average depth of approximately 273 m. We assume a halo length of 9 km. Using the same humidity as for the moisture mass-flux (as it is assumed that all the air advected upward is detraining). This leads to a mass of about $M_{\mathrm{detrained}} \approx 1.10 \cdot 10^{12}\,\mathrm{kg}$. Dividing these two estimations allows us to better quantify their difference: the ratio $M_{\mathrm{detrained}}/M_{\mathrm{wv}}$ is of the order $\mathcal{O}(10)$. Sensitivity tests indicate that variations in cloud lifetime, updraft strength, or assumed updraft width change the results only within the same order of magnitude, reinforcing the robustness of the conclusion.

Since the required detrained moisture exceeds what a typical updraft can supply—even under very favorable assumptions—it suggests that detrainment from a single cloud alone is insufficient to explain the observed increased humidity, suggesting that another mechanism must contribute (at least partially).

4.2. Methods: Vertical Profiles Composite

In light of these results, we hypothesize that shallow cumulus clouds and humidity anomalies are connected through mesoscale organization in the boundary layer, such that broader humidity patterns associated with cloud clustering help shape the spatial distribution of moisture and clouds. In this framework, we refer to localized humidity enhancements surrounding individual clouds as *humidity haloes*, emphasizing their cloud-scale

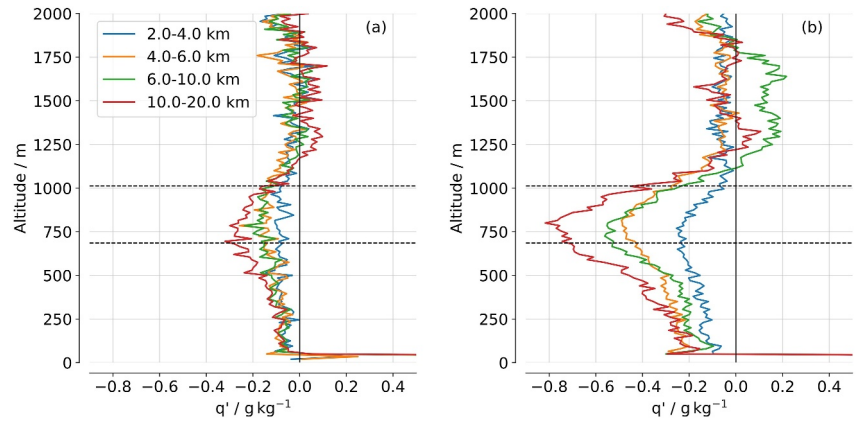

Figure 4. Specific humidity anomaly plotted for different (a) cloud distances and (b) gap lengths. In panel (a), vertical humidity profiles are shown relative to the mean profile for distances between 0 and 2 km; for example, the red line represents the anomaly for 10–20 km cloud distance. Panel (b) shows similar anomalies as a function of gap length, also relative to the 0–2 km reference. The horizontal black dashed lines show the mean cloud base and top height.

character, while *humidity anomalies* denote mesoscale variations that may reflect a degree of collective organization. Our goal is to assess the relative importance of these scales in modulating moisture variance at cloud level.

If clouds are the main source for increased humidity in their surrounding, one would expect the moistening to mostly decrease with the distance to the cloud boundary. To test this, we compute vertical profiles of specific humidity as a function of distance from the nearest cloud, averaging the profiles within predefined distance ranges. This approach allows us to isolate the contribution of individual clouds to local moisture levels. However, if clustering and mesoscale organization are the main drivers of humidity variability, we would expect clouds to cluster in areas of enhanced humidity. To that effect, we examine vertical humidity profiles across regions with varying gap lengths, defined as the distances between adjacent clouds. Small gap lengths correspond to denser cloud clustering, where humidity anomalies may overlap. Comparing humidity profiles across these gap-based regions allows us to distinguish whether moistening is dominated by individual cloud processes or by broader clustering patterns that may reflect mesoscale coherence in the boundary layer.

4.3. Results

Figure 4a shows vertical profiles of humidity at increasing distances from clouds, plotted relative to the closest distance bin (0–2 km), which serves as reference. All other profiles are drier than this reference, and humidity decreases progressively with distance from the clouds. This figure focuses on the effect of single clouds on forming a halo (from processes such as detrainment or lateral mixing). The differences are more pronounced within the cloud layer, particularly below approximately 1000 m—at the typical altitude range where shallow cumulus clouds are observed and slightly below, in the transition region. These results align with the findings of Albright et al. (2023), who also identified enhanced moisture variability around these altitudes.

Replacing distance from clouds by gap length (defined as the distance between two clouds) leads to Figure 4b. This figure shows that smaller gap lengths are moister relative to the 0−2 km reference. This pattern suggests that regions with smaller gaps, where clouds are closer together, are moister than larger gaps, where clouds are farther apart. As gap length increases, the profiles get (relatively) drier. Once again, the differences are more pronounced within the clouds, but also at lower altitude (around 250to 700 m). This enhancement at lower altitude is probably caused by a moister boundary layer in regions with high cloud concentration.

The most striking difference between the two panels of Figure 4 lies in the magnitude of humidity variations. Figure 4a shows differences of about 0.2 to 0.3 g kg^{-1} between the smallest distance bin (0–2 km) and the largest (10–20 km), while Figure 4b shows differences of up to 0.8 g kg^{-1}. This indicates that humidity variability increases with the degree of cloud clustering, suggesting that more closely spaced clouds are associated with stronger local moistening. The enhanced humidity gradients observed in Figure 4b challenge the initial intuitive

view—put forward in studies such as Gu et al. (2021), Lu et al. (2012), Perry and Hobbs (1996), and Wang and Geerts (2010)—that moisture haloes are primarily fed by single cloud detrainment (as sketched in Figure 1a). Our findings support the hypothesis that these humidity anomalies are shaped not only by individual cloud processes but also by patterns of cloud organization (see Figure 1b). This points to an emergent link between humidity haloes and cloud clustering.

5. Discussion and Conclusion

In this study, we analyzed humidity haloes surrounding trade wind shallow cumulus clouds using ground based measurements from the BCO. These haloes—regions of enhanced water vapor relative to the clear-sky—act as transition zones between dry air and clouds. Downward longwave radiation ($LW_\downarrow$) measurements revealed humidity haloes extending up to approximately 9 km from shallow cumulus clouds, with a mean RE of 0.68 W m^{-2}. This closely matches the 0.75 W m^{-2} reported by Eytan et al. (2020), using a completely different method, reinforcing the validity of our single-location measurement approach. Because earlier studies indicate that nearly half of the global clear-sky regions over the oceans occur within 5 km of low-level clouds (Bar-Or et al., 2011; Eytan et al., 2020; Varnai & Marshak, 2012), excluding near-cloud areas from water-vapor retrievals can systematically bias the observations toward drier atmospheric conditions.

Mass flux estimates suggest that the detrainment from a single shallow cloud cannot account for these humidity anomalies. LiDAR water vapor observations support the hypothesis that there is a relation between spatial clustering of cumuli and humidity decay away from the clouds. The moistening in the surrounding of clouds does not appear to arise solely from cloud detrainment (and therefore being an isolated product of single-cloud processes) but also from broader patterns of humidity that favor cloud clustering.

These interpretations are supported by Large Eddy Simulations findings. Janssens et al. (2024) demonstrated a two-way coupling between shallow convection and mesoscale circulations, whereby clouds and mesoscale motions tend to amplify one another and enhance moisture anomalies. Similarly, Bretherton and Blossey (2017) showed that shallow convection can self-aggregate into mesoscale patches. Our results provide observational evidence linking humidity haloes to spatial clustering and suggest that mesoscale organization may play a role in shaping the observed moisture variability.

Overall, our study advances understanding of humidity haloes' origin and role in the trade wind boundary layer, highlighting mesoscale dynamics' importance in shaping the cloud environment. It challenges the traditional view that humidity variations solely result from cloud processes, instead highlighting their connection to the spatial distribution and clustering of shallow cumuli, consistent with the conceptual framework of Janssens et al. (2024) and Vogel et al. (2022). Future work could benefit from new in situ observations, such as LiDAR from the HALO aircraft during the ORCESTRA campaign (Stevens et al., 2025), to further investigate halo properties. Large-eddy simulations could also test whether the observed humidity field between clouds can be reconstructed from the superposition of detraining clouds, helping to quantify the respective roles of cloud-scale and organizational processes. Exploring how different cloud types, including deeper convection, influence haloes characteristics—potentially leading to broader haloes through enhanced mixing and detrainment—could be pursued using the CORAL LiDAR at the BCO.

Conflict of Interest

The authors declare no conflicts of interest relevant to this study.

Data Availability Statement

All data used in this study were collected at the Barbados Cloud Observatory (BCO) and are accessible through the intake catalog (Stevens et al., 2016). Water vapor mixing ratio measurements were measured during the EUREC^{4}A campaign (Stevens et al., 2021). The EUREC^{4}A data is available and can be accessed via the intake catalog, as detailed in the documentation at https://howto.eurec4a.eu/intro.html. Processing code and plotting scripts are available via Rixen et al. (2025).

Acknowledgments
The authors thank the team managing the Barbados Cloud Observatory (BCO) at the Max Planck Institute for Meteorology and the Caribbean Institute for Meteorology and Hydrology for their dedicated maintenance of the site and for providing access to the data. Special thanks go to Ilya Serikov for his support with the BCO data and his clear explanations the CORAL Lidar which he developed and its data. Additionally Marius Rixen thanks Heini Wernli for his guidance and support on this project. The authors thank the reviewers for their valuable comments and suggestions. Open Access funding enabled and organized by Projekt DEAL.

References

Albright, A. L., Stevens, B., Bony, S., & Vogel, R. (2023). A new conceptual picture of the trade wind transition layer. *Journal of the Atmospheric Sciences*, *80*(6), 1547–1563. https://doi.org/10.1175/JAS-D-22-0184.1

Bar-Or, R. Z., Koren, I., Altaratz, O., & Fredj, E. (2012). Radiative properties of humidified aerosols in cloudy environment. *Atmospheric Research*, *118*, 280–294. https://doi.org/10.1016/j.atmosres.2012.07.014

Bar-Or, R. Z., Altaratz, O., & Koren, I. (2011). Global analysis of cloud field coverage and radiative properties, using morphological methods and MODIS observations. *Atmospheric Chemistry and Physics*, *11*(1), 191–200. https://doi.org/10.5194/acp-11-191-2011

Bretherton, C. S., & Blossey, P. N. (2017). Understanding mesoscale aggregation of shallow cumulus convection using large-eddy simulation. *Journal of Advances in Modeling Earth Systems*, *9*(8), 2798–2821. https://doi.org/10.1002/2017MS000981

Eytan, E., Koren, I., Ronen, A., & Kostinski, A. B. (2020). Longwave radiative effect of the cloud twilight zone. *Nature Geoscience*, *13*(10), 669–673. https://doi.org/10.1038/s41561-020-0636-8

George, G., Stevens, B., Bony, S., Vogel, R., & Naumann, A. K. (2023). Widespread shallow mesoscale circulations observed in the trades. *Nature Geoscience*, *16*(7), 584–589. https://doi.org/10.1038/s41561-023-01215-1

Gonzalez, J.-A., Calbo, J., & Sola, Y. (2023). Assessment of cloudless-to-cloud transition zone from downwelling longwave irradiance measurements. *Atmospheric Research*, *285*, 106657. https://doi.org/10.1016/j.atmosres.2023.106657

Gu, J.-F., Plant, R. S., Holloway, C. E., & Jones, T. R. (2021). Composited structure of non-precipitating shallow cumulus clouds. *Quarterly Journal of the Royal Meteorological Society*, *147*(738), 2818–2833. https://doi.org/10.1002/qj.4101

Jahani, B., Calbo, J., & Gonzalez, J.-A. (2020). Quantifying transition zone radiative effects in longwave radiation parameterizations. *Geophysical Research Letters*, *47*(22), e2020GL090408. https://doi.org/10.1029/2020GL090408

Janssens, M., George, G., Schulz, H., Couvreux, F., & Bouniol, D. (2024). Shallow convective heating in weak temperature gradient balance explains mesoscale vertical motions in the trades. *Journal of Geophysical Research: Atmospheres*, *129*(18), e2024JD041417. https://doi.org/10.1029/2024JD041417

Jung, E., Albrecht, B. A., Feingold, G., Jonsson, H. H., Chuang, P., & Donaher, S. L. (2016). Aerosols, clouds, and precipitation in the North Atlantic trades observed during the Barbados aerosol cloud experiment – Part 1: Distributions and variability. *Atmospheric Chemistry and Physics*, *16*(13), 8643–8666. https://doi.org/10.5194/acp-16-8643-2016

Konow, H. (2020). BCO cloudmask code. *Zenodo*. https://doi.org/10.5281/zenodo.4312818

Lonitz, K. (2014). *Susceptibility of trade wind cumulus clouds to precipitation*. (Unpublished doctoral dissertation). Universität Hamburg Hamburg.

Lu, C., Liu, Y., Niu, S., & Vogelmann, A. M. (2012). Lateral entrainment rate in shallow cumuli: Dependence on dry air sources and probability density functions. *Geophysical Research Letters*, *39*(20), L20812. https://doi.org/10.1029/2012GL053646

Malkus, J. S. (1954). Some results of a trade-cumulus cloud investigation. *Journal of the Atmospheric Sciences*. Retrieved from https://journals.ametsoc.org/view/journals/atsc/11/3/1520-0469_1954_011_0220_sroatc_2_0_co_2.xml

Medeiros, B., & Nuijens, L. (2016). Clouds at Barbados are representative of clouds across the trade wind regions in observations and climate models. *Proceedings of the National Academy of Sciences of the United States of America*, *113*(22), E3062–E3070. https://doi.org/10.1073/pnas.1521494113

Perry, K. D., & Hobbs, P. V. (1996). Influences of isolated cumulus clouds on the humidity of their surroundings. *Journal of the Atmospheric Sciences*, *53*(1), 159–174. https://doi.org/10.1175/1520-0469(1996)053<0159:ioicco>2.0.co;2

Pinsky, M., & Khain, A. (2019). Theoretical analysis of the entrainment–mixing process at cloud boundaries. Part II: Motion of cloud interface. *Journal of the Atmospheric Sciences*, *76*(8), 2599–2616. https://doi.org/10.1175/JAS-D-18-0314.1

Rixen, M., Windmiller, J., & Stevens, B. (2025). Dataset for: "influence of mesoscale circulations on the formation humidity haloes". https://doi.org/10.5281/zenodo.16961150

Siebesma, A. P., Bretherton, C. S., Brown, A., Chlond, A., Cuxart, J., Duynkerke, P. G., et al. (2003). A large eddy simulation intercomparison study of shallow cumulus convection. *Journal of the Atmospheric Sciences*, *60*(10), 1201–1219. https://doi.org/10.1175/1520-0469(2003)60⟨1201:ALESIS⟩2.0.CO;2

Stevens, B., Bony, S., David, R., Delanoë, J., Gross, S., Klocke, D., et al. (2025). *Orcestra: Organized convection and earthcare studies over the tropical Atlantic*. Tellus.

Stevens, B., Bony, S., Farrell, D., Ament, F., Blyth, A., Fairall, C., et al. (2021). EUREC4A. *Earth System Science Data*, *13*(8), 4067–4119. https://doi.org/10.5194/essd-13-4067-2021

Stevens, B., Farrell, D., Hirsch, L., Jansen, F., Nuijens, L., Serikov, I., et al. (2016). The Barbados cloud observatory—Anchoring investigations of clouds and circulation on the edge of the ITCZ. *Bulletin of the American Meteorological Society*, *97*(5), 787–801. https://doi.org/10.1175/BAMS-D-14-00247.1

Varnai, T., & Marshak, A. (2012). Analysis of co-located MODIS and CALIPSO observations near clouds. *Atmospheric Measurement Techniques*, *5*(2), 389–396. https://doi.org/10.5194/amt-5-389-2012

Vogel, R., Albright, A. L., Vial, J., George, G., Stevens, B., & Bony, S. (2022). Strong cloud–circulation coupling explains weak trade cumulus feedback. *Nature*, *612*(7941), 696–700. https://doi.org/10.1038/s41586-022-05364-y

Wang, Y., & Geerts, B. (2010). Humidity variations across the edge of trade wind cumuli: Observations and dynamical implications. *Atmospheric Research*, *97*(1), 144–156. https://doi.org/10.1016/j.atmosres.2010.03.017